Evaluation of component interface quality in 3D micro-CT images of metallurgical coke

D. R. Jenkins[1] Ai Wang[2]

(Received 31 January 2023; revised 10 February 2024)

Abstract

Metallurgical coke is a crucial component in the production of steel worldwide. It is a porous composite material, created by conversion of metallurgical coal in a coke oven. A key property of metallurgical coke is its strength, and there is evidence that poor interface quality between the two key components of coke can have deleterious effect on coke strength. Here we create small samples of coke and image them using high resolution 3D micro-CT, with pixel size of approximately 8 µm. We use a Gabor filter, combined with morphology techniques to isolate the different components in the samples. We then develop a measure, called excess porosity to quantify the quality of the interfaces between components. This measure enables us to highlight problem interactions between components.

DOI:10.21914/anziamj.v64.17972, Published 2024-04-09, as part of the Proceedings of the 20th Biennial Computational Techniques and Applications Conference. ISSN 1445-8810. (Print two pages per sheet of paper.)

Contents

1 Introduction

Metallurgical coke is a porous composite material. In simple terms, the material consists of mineral matter (a few percent of the volume), pores (30–50%) and two different carbon phases: *reactive maceral derived components* (RMDC) and *inert derived maceral components* (IMDC). RMDC is a highly porous phase, while IMDC is more solid. The amount, size and distribution of IMDC particles throughout the coke microstructure is a key determinant of coke strength, which is important for its performance in the blast furnace. Recent studies [2, 12] investigated the role that the interfaces between IMDC and RMDC in the coke structure play in affecting its strength. The size distribution and mass/volume fraction of inerts clearly affect coke strength. It has been demonstrated that coke breakage, in terms of crack propagation, has a tendency to follow around the outer surfaces of inerts, or through pre-existing internal flaws of inerts [10]. This implies that the quality of the bonding between IMDC and RMDC is important in determination of coke strength—so-called 'adhesion controlled' strength [5].

Other approaches to investigating the IMDC-RMDC interactions include those of Barranco et al. [1], Barriocanal et al. [3, 4, 2], Kubota et al. [7, 8] and

Saito et al. [13]. Fractographic approaches by Roest et al. [12] have also been used. In particular, Roest et al. [12] identified the porosity at the IMDC-RMDC interface in coke as a critical parameter contributing to coke failure at tuyere regions. Most of these studies have relied on destructive testing of coke samples—either polishing surfaces for microscopy or applying loads in various forms to create fracture surfaces for examination. The load associated with forming such fractures is generally extremely large, at least compared to typical loads that might be expected for coke lumps within a blast furnace. In our study, micro-CT analysis is non-destructive and is not associated with the application of potentially unrealistic loads. Moreover, our analysis considers the whole 3D surface of inerts, rather than a 2D slice or a portion of an inert surface that has been involved in a fracture.

The aim is to develop a comprehensive set of analysis tools for characterising the IMDC-RMDC interface using micro-CT images. The main focus here is to develop a simple measure to quantify the quality of the IMDC-RMDC interface.

2 Samples and imaging

Coal samples were prepared by performing a maceral separation step, to obtain vitrinite-rich and inertinite-rich components. Vitrinite is the 'reactive' component of coal, which softens and resolidifies during coking, creating the RMDC, while inertinite hardly changes during coking, forming IMDC. Vitrinite was crushed using mortar and pestle to less than 1 mm size. Three inertinite particles of size 2–3 mm were chosen by hand for each sample. The crucibles were half filled with vitrinite, then the three inertinite particles were carefully placed equal distances apart (Figure 1(a)), then the crucible was filled to the top with vitrinite. Each sample had a total mass of 0.5 g. The graphite crucibles have approximate internal dimension of $16 \times 6 \times 7$ mm, 2 mm thick walls and the lids have a 1 mm inset. The samples were then coked (heated in the absence of air to 1000°C at 3°C per minute) (Figure 1(b)), cooled and then sent for micro-CT imaging. Because we studied the interaction of components from different coals, a total of 55 samples were prepared, coked

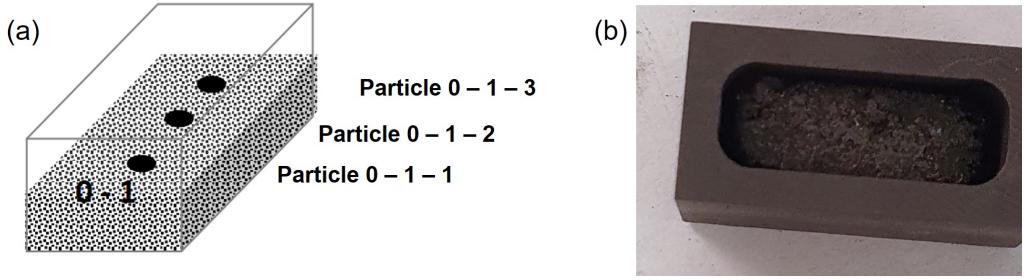

Figure 1: (a) schematic of filling of sample with vitrinite and inertinite particles; (b) coked sample. The three IMDC particles are not visible in the coke sample because they are embedded within.

and imaged.

Imaging was carried out at the Imaging and Medical Beamline (IMBL) at the Australian Synchrotron, part of ANSTO, in Clayton, Victoria. The beamline provides high resolution 3D micro-CT images, in our case with a pixel size of about 8 μm. Overall, the total amount of data received from the IMBL imaging was several terabytes, which needed to be processed then analysed.

3 Image analysis

Re-constructed images for each sample comprised around 1200 32-bit tif files, one for each slice. Each file is about 54.3 Mb in size and a total of around 64 Gb for the full stack of images. For consistency, initial processing was performed to rotate each image and crop to remove the crucible. The cropped images were 5.3 Mb in size—only 10% of the original images.

From Figure 3 it is relatively easy to identify, by eye, the location of the three large IMDC particles in the samples. However, the challenge is to actually identify, as accurately as possible, the location of the IMDC-RMDC interface. A key issue is that the IMDC particles have approximately the same 'density'

as the RMDC material in the micro-CT images, as measured by greyscale intensity due to X-ray absorption, because both components consist mainly of carbon. So it is not possible to distinguish IMDC from RMDC based on the greyscale intensity. Instead, we use the differing 'texture' between the IMDC (usually relatively smooth) and the RMDC (usually porous with a reasonably well-defined pore/pore wall structure of relatively consistent dimensions). The tool we use for doing the texture analysis is a Gabor filter [6], which is a locally compact, wavelet type of filter, being the combination of a sine wave within a Gaussian envelope:

$$G(x, y) = \frac{1}{\pi} \exp\left(\frac{x'^2 + y'^2}{2\sigma^2}\right) \exp\left(2\pi f x\right), \tag{1}$$

where

$$x' = x\cos\theta + y\sin\theta, \quad y' = -x\sin\theta + y\cos\theta,$$

and where x and y are the coordinates of the image plane, σ is the standard deviation of the Gaussian envelope and θ is the orientation of the normal to the parallel stripes of a Gabor function. The filter has a characteristic spatial scale f, and the scale needs to be adjusted for each sample to obtain the best response from the filter, as the porosity can differ from sample to sample. The Gabor filter approach to coke image analysis was previously developed by CSIRO Data61 [9].

The following steps are carried out for IMDC identification, for each sample.

1. Threshold the cropped images into solid and pore phase. A standard Otsu thresholding approach was used [11].
2. Use a characteristic (vertical xz plane) slice (usually about halfway across the sample) to find the best scale f to give the largest response for the filter. The filter is applied at 10 different orientation angles θ with an increment of 18°, and the responses are added together.

3. Calculate the Gabor filter response for each of the 1200 slices in the image, using the chosen scale, again using the sum of responses from 10 orientations.
4. Threshold the response images, using the Otsu method, to find the location of the IMDC.
5. Using the AND logical operator, combine the result with the original thresholded image from Step 1, to eliminate pores from the response.
6. Re-slice the original image stack in the two other planes (xy and yz planes) and repeat Steps 3, 4 and 5 for those planes.
7. Using the OR operator, combine the responses for the three different plane directions to obtain an overall response to the filter.
8. 3D morphological closing and opening are applied to the overall response image to reduce pore wall connections to the targeted inert particles. The size structuring element depends on the thickness of pore wall and varies in each sample.
9. Find the three largest connected entities (IMDC particles) in the overall response image. These are the identified IMDC (note sometimes less than three, if one or more of the particles has fused).
10. Use 3D mathematical morphology operations (opening and closing) to further clean the images, break connections where they should not exist and use dilation and erosion to fill holes in the body of the IMDC.

The result provides a 3D mask for each IMDC particle in the sample. In some cases, the mask is eroded by one or two pixels, to ensure that it does not overlap the surface of the IMDC particle. For our purposes, it is better that the mask is slightly within the bounds of the particle, rather than exceeding the bounds. The computation time for analyzing each sample is around four hours on a high performance workstation.

The standard procedure described here did not provide a satisfactory mask

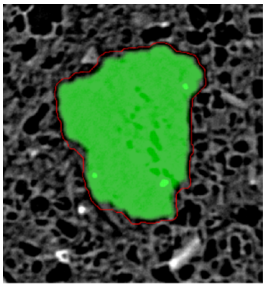

Figure 2: a single pixel-wide band (red line) at maximum porosity position around an IMDC particle.

for IMDC for 23 particles, out of the almost 150 that were analysed. These 23 particles were all of a type that have a significant fraction of 'internal porosity', where the internal volume of the particle contained some porous, apparently fused material. In most cases, the particles are 'layered', with alternating porous and solid components. In order to better identify the boundary of such particles, we modify the Gabor filter approach in one way—we identify the predominant angle of the solid fractions of the particle and collected a set of 11 Gabor filter results in a band of $\pm 50°$ about that angle, and then add them together. This results in an improved total response to the Gabor filter, because the original approach would have potentially zero response for the angles that were out of alignment with the direction of the solid fragments. The significant angles are identified in all three planes, and the filter step applied in each plane. Some additional mathematical morphology operations are implemented to fill the gaps between the solid pieces. Ultimately, there are seven particles where the particle identification remains unsatisfactory.

Once the IMDC particle mask is identified, we produce a distance map—a 3D pixel array that records the perpendicular Euclidean distance from the surface of the mask of each IMDC particle. Then we create a series of concentric shells, 1 pixel ($\sim 8\,\mu m$) thick, emanating outward from the surface of the IMDC particle mask. The bounds of the ith shell, being i pixels from the surface, were set at $i - 0.5$ and $i + 0.5$ pixels, using thresholding. The shells are used to calculate average values of quantities of interest, at set distances from the particle surface. Figure 2 shows an image of a single slice, with a

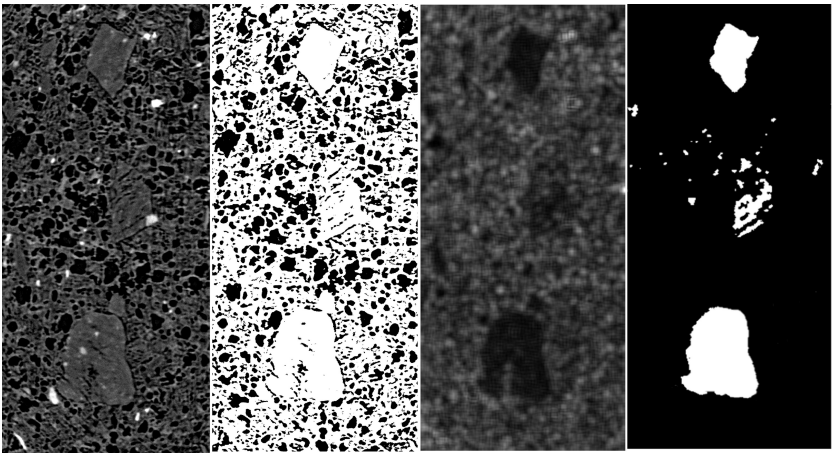

Figure 3: (from left to right) original image, thresholded image, Gabor filter response, and post-morphological operations.

single pixel wide shell approximately 10 pixels away from the mask.

We use the calculated shells to calculate the average porosity of each sample, at increasing distances away from the surface of each identified IMDC particle. Thresholded (solid-pore) images are used for this calculation. This gives a profile of porosity variation from (just inside) the surface of the IMDC particle, to a distance away from the particle where the pore structure is unaffected by the presence of the particle—typically a distance of 1 mm. Going further risks becoming too close to a neighbouring particle or the outer surface of the sample. The *excess porosity* is defined as the porosity of the first peak nearest the particle surface minus the average porosity at some distance ~ 500–1000 µm from the particle mask surface.

4 Sample results

Figure 3 shows the individual steps in the IMDC identification process: (a) a cropped and rotated image; (b) thresholded image; (c) Gabor filter reponse

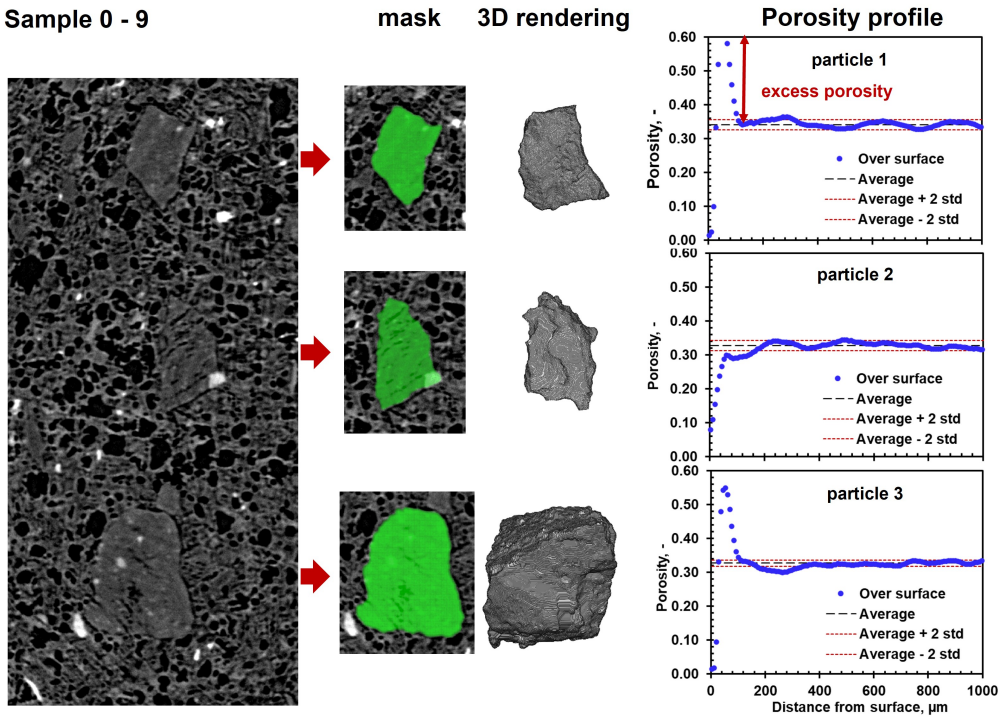

Figure 4: summary of results for one sample.

map; and (d) a thresholded and processed set of masks for the three IMDC particles. We observe that the middle particle is not well resolved, as it contains more internal porosity than the other two particles, but this is one of the particles where we adopt the modified approach. Ultimately, the result is good for that particle also, as is shown in the results of Figure 4. This figure also shows the variation of porosity obtained from the shell analysis, and the difference between the excess porosity of the middle particle, compared with the other two particles. The implication from this result is that the middle particle is well bound into the microstructure of the coke, whereas the other two particles are not. This is key information for understanding the IMDC-RMDC interface behaviour.

5 Conclusions

This work shows that (a) using the image analysis tools based around the Gabor filter, we quite accurately distinguish RMDC-IMDC interfacial region for coke samples, and (b) using a shell analysis to determine the excess porosity, so as to obtain a sensible measure to quantify the quality of the interface. In essence, this work presents a means of distilling the large amount of information present in a 3D micro-CT image to a single quantity of importance. The next step is to use this measure to evaluate the quality of IMDC-RMDC interfaces for a range of different combinations of coal components, and relate these measures to the strength of coke produced using such combinations. The latter requires either experimental measures of coke strength, or solution of mechanical equilibrium equations for the complex microstructures produced in this study, both of which are the targets of further work. The use of 3D micro-CT imaging in materials analysis is expanding rapidly, producing large amounts of data that need to be analysed. It is expected that the methods described here could prove useful when applied to images of other materials.

6 Acknowledgements

The authors acknowledge funding for this project from the Australian Coal Association Research Program, under ACARP Project C33063.

The authors acknowledge merit-based access to the IMBL at the Australian Synchrotron, Reference No: AS213/IMBL/17518, and thank the beamline scientists for performing the imaging due to Covid constraints.

The authors acknowledge guidance and assistance from colleagues at NIER, University of Newcastle, in preparation of samples. Coal samples were supplied by Tata Steel Europe.

References

[1] R. Barranco, J. Patrick, C. Snape, and A. Thompson. "Impact of low-cost filler material on coke quality". In: *Fuel* 86.14 (2007), pp. 2179–2185. DOI: 10.1016/j.fuel.2007.03.013 (cit. on p. C149).

[2] C. Barriocanal, S. Hanson, J. W. Patrick, and A. Walker. "Reactive-inert interfaces in metallurgical cokes: Effect of added inerts". In: *Fuel* 75.2 (1996), pp. 243–245. DOI: 10.1016/0016-2361(95)00233-2 (cit. on p. C149).

[3] C. Barriocanal, S. Hanson, J. W. Patrick, and A. Walker. "The characterization of interfaces between textural components in metallurgical cokes". In: *Fuel* 73.12 (1994), pp. 1842–1847. DOI: 10.1016/0016-2361(94)90209-7 (cit. on p. C149).

[4] C. Barriocanal, S. Hanson, J. W. Patrick, and A. Walker. "The quality of interfaces in metallurgical cokes containing petroleum coke". In: *Fuel Proces. Tech.* 45 (1995), pp. 1–10. DOI: 10.1016/0378-3820(95)00003-P (cit. on p. C149).

[5] P. Bennett, F. Shi, and N. Andriopoulos. "Determination of a theoretically based coke strength index or indices based on drum tests". In: *ACARP Project C20009* (2013). URL: https://www.acarp.com.au/abstracts.aspx?repId=C20009 (cit. on p. C149).

[6] M. Haghighat, S. Zonouz, and M. Abdel-Mottaleb. "CloudID: Trustworthy cloud-based and cross-enterprise biometric identification". In: *Expert Sys. Appl.* 42 (2015), pp. 7905–7916. DOI: 10.1016/j.eswa.2015.06.025 (cit. on p. C152).

[7] T. Kanai, Y. Yamazaki, X. Zhang, A. Uchida, Y. Saito, M. Shoji, H. Aoki, S. Nomura, Y. Kubota, H. Hayashizaki, and S. Miyashita. "Quantification of the existence ratio of non-adhesion grain boundaries and factors governing the strength of coke containing low-quality coal".

In: *J. Therm. Sci. Tech.* 7.2 (2012), pp. 351–363. DOI: 10.1299/jtst.7.351 (cit. on p. C149).

[8] Y. Kubota, S. Nomura, T. Arima, and K. Kato. "Effects of coal inertinite size on coke strength". In: *ISIJ Int.* 48.5 (2008), pp. 563–571. DOI: 10.2355/isijinternational.48.563 (cit. on p. C149).

[9] R. Li, D. R. Jenkins, and R. Pearce. "Texture-based identification of inert-maceral derived components in metallurgical coke". In: *MODSIM* (2015). URL: https://www.mssanz.org.au/modsim2015/A1/li_r.pdf (cit. on p. C152).

[10] H. Lomas, D. R. Jenkins, M. R. Mahoney, R. Pearce, R. Roest, K. Steel, and S. Mayo. "Examining mechanisms of metallurgical coke fracture using micro-CT imaging and analysis". In: *Fuel Proc. Tech.* 155 (2017), pp. 183–190. DOI: 10.1016/j.fuproc.2016.05.039 (cit. on p. C149).

[11] N. Otsu. "A threshold selection method from gray-level histograms". In: *IEEE Trans. Sys. Man. Cyber* 9 (1979), pp. 62–66. DOI: 10.1109/TSMC.1979.4310076 (cit. on p. C152).

[12] R. Roest, H. Lomas, S. Gupta, R. Kanniala, and M. R. Mahoney. "Fractographic approach to metallurgical coke failure analysis. Part 3: Characterisation of fracture mechanisms in a blast furnace coke". In: *Fuel* 180 (2016), pp. 803–812. DOI: 10.1016/j.fuel.2016.04.019 (cit. on pp. C149, C150).

[13] Y. Saito, T. Kanai, D. Igawa, Y. Miyamoto, S. Matsuo, Y. Matsushita, H. Aoki, S. Nomura, H. Hayashizaki, and S. Miyashita. "Image recognition method for defect on coke with low-quality coal". In: *ISIJ Int.* 54.11 (2014), pp. 2512–2518. DOI: 10.2355/isijinternational.54.2512 (cit. on p. C150).

Author addresses

1. **D. R. Jenkins**, NIER, University of Newcastle, Callaghan, NSW 2308, Australia.
   mailto:David.Jenkins@newcastle.edu.au
2. **Ai Wang**, NIER, University of Newcastle, Callaghan, NSW 2308, Australia.